Nanoscale

RSC Publishing

PAPER

View Article Online
View Journal | View Issue

Cite this: *Nanoscale*, 2013, **5**, 3428

Textile electrodes woven by carbon nanotube–graphene hybrid fibers for flexible electrochemical capacitors†

Huhu Cheng,[a] Zelin Dong,[a] Chuangang Hu,[a] Yang Zhao,[a] Yue Hu,[a] Liangti Qu,*[a] Nan Chen[a] and Liming Dai*[b]

Received 18th January 2013
Accepted 19th February 2013

DOI: 10.1039/c3nr00320e

www.rsc.org/nanoscale

Functional graphene-based fibers are promising as new types of flexible building blocks for the construction of wearable architectures and devices. Unique one-dimensional (1D) carbon nanotubes (CNTs) and 2D graphene (CNT/G) hybrid fibers with a large surface area and high electrical conductivity have been achieved by pre-intercalating graphene fibers with Fe_3O_4 nanoparticles for subsequent CVD growth of CNTs. The CNT/G hybrid fibers can be further woven into textile electrodes for the construction of flexible supercapacitors with a high tolerance to the repeated bending cycles. Various other applications, such as catalysis, separation, and adsorption, can be envisioned for the CNT/G hybrid fibers.

1 Introduction

Graphene with a two dimensional (2D) carbon nanostructure has fascinating properties, including giant electron mobility, large surface area, high mechanical, thermal and chemical stability.[1–5] As a consequence, many attempts have been made to integrate the unique properties of the individual graphene sheets into useful 1D fibers, 2D films and 3D graphene ensembles for practical applications.[6,7] Some breakthroughs have recently been made for the fabrication of 1D macroscopic graphene fibers (GFs) *via* wet-spinning by several groups,[8,9] and through hydrothermal strategy by us.[10,11] The resultant GFs are light-weight, highly flexible, and electro-conductive. Due to the strong π–π stacking interaction between individual graphene sheets,[12,13] however, the unique 2D feature such as the initial large surface area of graphene sheets would be drastically lost during the manufacturing process, which largely limits their applications in certain devices that specifically require large surface areas (*e.g.*, supercapacitors).

As a member of the carbon family, 1D carbon nanotubes (CNTs) also possess unique properties.[14–17] Recent studies demonstrate that hybrid materials of the 2D graphene sheets and 1D CNTs can exhibit synergistic effects to show greatly improved electrical, thermal conductivity and mechanical flexibility compared with each of the single constituent components.[18–23] So far, some of such 2D and 3D hybrid structures have been fabricated as transparent conductors[19] and electrode materials for supercapacitors.[22,24] However, the fabrication of 1D macroscopic CNT/graphene (CNT/G) hybrid fibers has been much less discussed, though they are promising as new types of flexible building blocks for the construction of wearable architectures and devices. By solution spinning of graphene and CNTs with poly(vinyl alcohol) (PVA), Min *et al.*[25] have recently produced hybrid fibers with much increased toughness. However, the high surface area and conductivity intrinsically associated with graphene and CNTs have been significantly reduced by the presence of the intercalated polymers.

Electrochemical capacitors (ECs) have attracted much attention because of their high power density, long cycle life, and high charge-storage efficiency.[26–32] Of particular interest is the development of lightweight, flexible supercapacitors[33] that have high capacitance performances even under mechanical deformation. We have recently demonstrated extremely high capacitances for 3D graphene structures with highly exposed graphene planar surfaces,[34] and highly compression-tolerant supercapacitors for graphene-based foam electrodes.[35] In this study, we have developed a flexible EC with textile electrodes made from CNT/G hybrid fibers of large surface area and high flexibility. The CNT/G hybrid fibers were fabricated by directly growing CNTs along graphene fibers with embedded Fe_3O_4 nanoparticles as catalysts for chemical vapor deposition (CVD) of the nanotubes.

2 Experimental

2.1 Preparation of CNT/G fibers

A graphene oxide (GO) suspension was prepared by a modified Hummers method as reported in our previous papers.[10,33,35] The Fe_3O_4-containing graphene (G/Fe_3O_4) fiber was obtained by thermally treating the mixture of 8 mg ml^{-1} GO and Fe_3O_4

[a]*Key Laboratory of Cluster Science, Ministry of Education of China, School of Chemistry, Beijing Institute of Technology, Beijing 100081, P.R. China. E-mail: lqu@bit.edu.cn; Fax: +86 10 68918608; Tel: +86 10 68918608*

[b]*Department of Macromolecular Science and Engineering, Case School of Engineering, Case Western Reserve University, 10900 Euclid Avenue, Cleveland, Ohio 44106, USA. E-mail: liming.dai@case.edu*

† Electronic supplementary information (ESI) available: Electrochemical measurement of graphene fibers. See DOI: 10.1039/c3nr00320e

nanoparticles (20 nm, Aladdin Chemistry Co. Ltd) in a closed glass pipeline[10] (Fig. 1). The weight ratio of GO suspension/Fe_3O_4 is 4 : 1. Then, we transfer the G/Fe_3O_4 fiber into a CVD chamber for the CNT growth. The fabrication of the CNT/G fiber was carried out at 750 °C under a flow of C_2H_2/H_2/Argon (5 sccm/150 sccm/800 sccm) for 15 min.

2.2 Preparation of a flexible supercapacitor

The textile electrodes were fabricated by pre-weaving the G/Fe_3O_4 fibers, followed by the CVD process as mentioned above. Thin polyethylene terephthalate (PET) films coated with an Au layer were used as supporting substrates and current collectors. The separator is a filter paper soaked with 1 M Na_2SO_4 aqueous electrolyte.

2.3 Characterization

The morphology of the samples was examined by scanning (SEM, JSM-7001F) and transmission (TEM, JEM-2010) electron microscopies. The X-ray energy disperse spectra (EDS) of the samples were taken on a JSM-7001F SEM unit. The Raman spectra were measured under ambient conditions using a Renishaw microRaman spectroscopy system with a 514.5 nm argon-ion laser. The X-ray diffraction (XRD) patterns were obtained by using a Netherlands 1710 diffractometer with a Cu Kα irradiation source ($\lambda = 1.54$ Å). The electrical conductivity of the CNT/G fiber was measured by using a four-probe resistance tester (Model ST2258A, Suzhou, China). A mechanical property test of the CNT/G fiber was conducted with an AGS-X material testing system (SHIMADZU). The strain rate for one centimeter gauge length is 0.2 mm min^{-1} with a preload of 0.5 N. Cyclic voltammetry (CV) and galvanostatic charge–discharge curves were recorded using a CHI 660D electrochemical workstation.

3 Results and discussion

Fig. 1 schematically shows the process for fabricating CNT/G fibers. Briefly, the aqueous GO suspension (8 mg ml^{-1}) was well mixed with Fe_3O_4 nanoparticles under ultrasonication, followed by a hydrothermal process within glass pipelines according to our previous report.[10] Graphene/Fe_3O_4 (G/Fe_3O_4) fibers were collected after being released from the pipelines, which were then treated through the CVD process for direct growth of CNTs along graphene fibers.

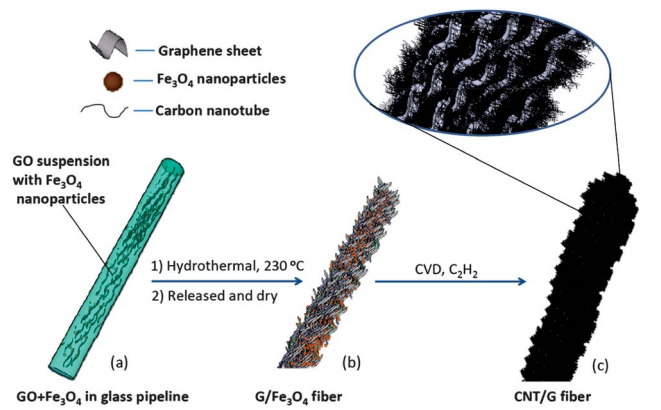

Fig. 1 Fabrication scheme of the CNT/G fibers. (a) An aqueous GO suspension mixed with Fe_3O_4 nanoparticles in a closed glass pipeline. (b) The G/Fe_3O_4 fiber released from the pipelines and dried after the hydrothermal process. (c) The as-prepared fluffy CNT/G fiber with the enlarged schematic drawing showing CNTs grown between graphene sheets after the CVD process.

Just like the pristine graphene fibers,[10] the as-prepared G/Fe_3O_4 fiber (Fig. 2a, left) has a uniform diameter of ~34 μm (Fig. 2b) and is composed of densely packed graphene sheets (Fig. 2b and c). A high-magnification cross-sectional SEM image of the G/Fe_3O_4 fiber reveals the intercalation of Fe_3O_4 nanoparticles within graphene sheets (Fig. 2d). O and Fe elemental mappings (Fig. 2f and g) are consistent with the C mapping (Fig. 2e) determined by EDS, indicating the uniform distribution of Fe_3O_4 along the graphene fiber.

The CNT/G fiber was prepared by the CVD process carried out at 750 °C under a flow of C_2H_2/H_2/Argon (5 sccm/150 sccm/800 sccm) for 15 min, which almost maintained the initial length of the G/Fe_3O_4 fiber (Fig. 2a, right), while its diameter increased significantly. Fig. 2h exhibits a CNT/G fiber with a diameter of 100 μm, about three times that of the G/Fe_3O_4 fiber. The observed fluffy surface of the CNT/G fiber (Fig. 2h) is composed of highly entangled CNTs (Fig. 2i). Fig. 2j and k show the cross-sectional view of a deliberately broken CNT/G fiber, which indicates that the CNTs grew not only on the surface but also within the fiber to increase the fiber diameter. The CNT/G fiber maintains the good flexibility of the graphene fiber, as demonstrated by bending it into a loop (Fig. 2l) or spring shape (Fig. 2m) without any obvious structural damage. Due to the expansion of the densely packed graphene sheets by the intercalated growth of CNTs, the CNT/G fiber has a lower tensile strength (24.5 MPa) than that of a pure graphene fiber (180 MPa).[10] As a consequence, we have observed the relatively large specific surface area of the CNT/G fibers (*ca.* 79.5 $m^2 g^{-1}$), which is close to the theoretical specific surface area of multi-wall carbon nanotubes,[36] but is significantly higher than that of pure graphene fibers (*ca.* 18 $m^2 g^{-1}$). Furthermore, the CNT/G fiber has a four-probe electrical conductivity of about 12 S cm^{-1} at room temperature, which is also slightly higher than that of graphene fiber (*ca.* 10 S cm^{-1}), probably attributable to the highly entangled CNTs within fibers and efficient electric transport between graphene sheets and CNTs.[10,20,22]

Despite the difficulty in observing the graphene sheets by SEM, Fig. 2h–k due to the dense growth of CNTs, the hybrid structure of CNTs with graphene sheets was confirmed by TEM imaging (Fig. 3a and b). The inset in Fig. 3b shows the typical electron diffraction pattern of a highly crystalline graphene sheet. The multiwalled graphitic layers are clearly observed in the high resolution TEM image of the grown CNT in Fig. 3c. Since the Fe_3O_4 nanoparticles were pre-anchored on the graphene sheets during the synthesis of the G/Fe_3O_4 fiber, it seems that the CNTs grow out from the nucleation catalysts distributing along the graphene planar sheets (Fig. 3d). The enlarged view of the nucleation site is presented in the inset of Fig. 3d, which displays the metal core surrounded by graphitic layers. The catalyst is not removed after the growth of CNTs, which has a low content of less than 2 wt% within G/CNT fibers (Fig. S1 in

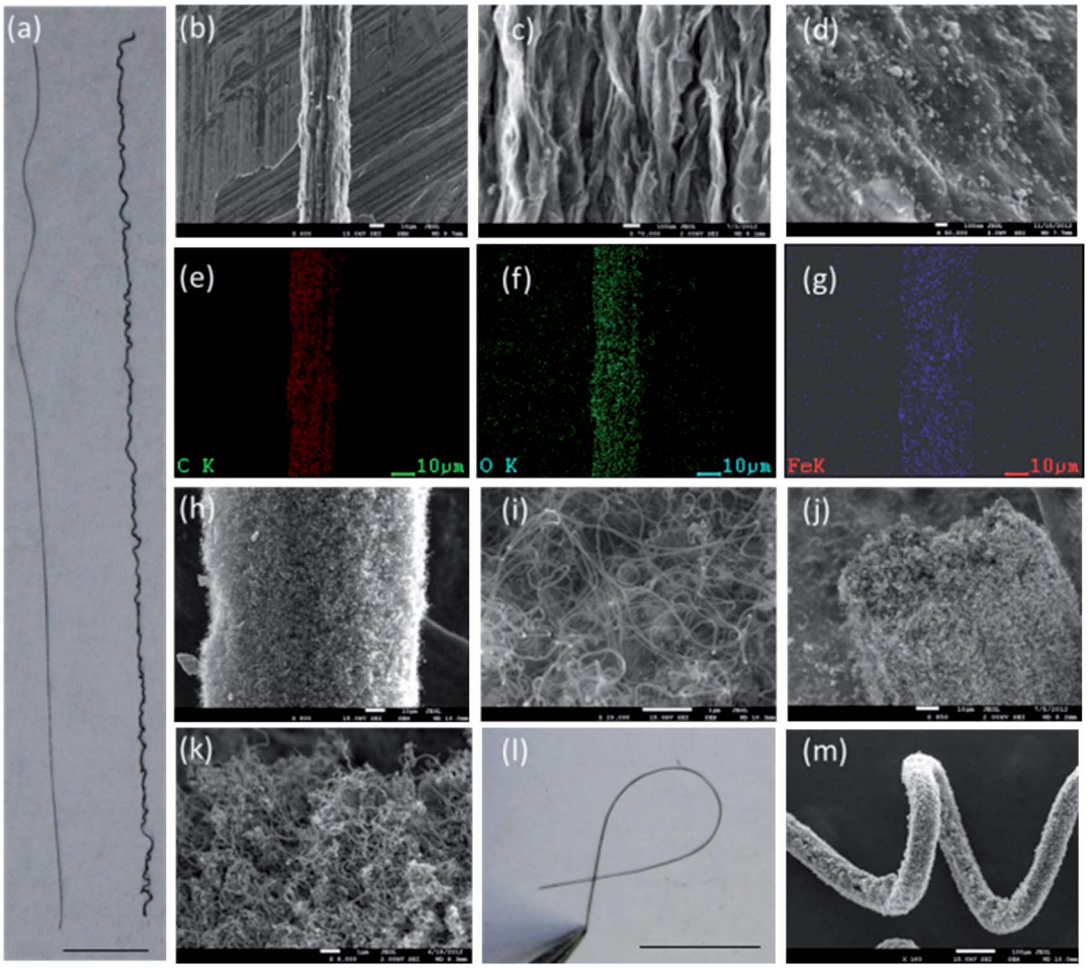

Fig. 2 (a) Photograph of an ~5 cm long G/Fe_3O_4 fiber (left) and a CNT/G fiber (right). (b) SEM image of the G/Fe_3O_4 fiber. (c and d) The surface and cross-sectional SEM images of the G/Fe_3O_4 fiber, respectively. (e–g) C, O, and Fe elemental mappings of (b) determined by EDS. (h and i) SEM images of the G/CNT fiber and enlarged surface, respectively. (j and k) Cross-sectional view of the CNT/G fiber with different magnifications. (l) A photo of a loop shaped CNT/G fiber. (m) The spring shape of the CNT/G fiber. Scale bars: a, 0.5 cm; b, h and j, 10 μm; c and d, 100 nm; i and k, 1 μm; l, 1 cm; m, 100 μm.

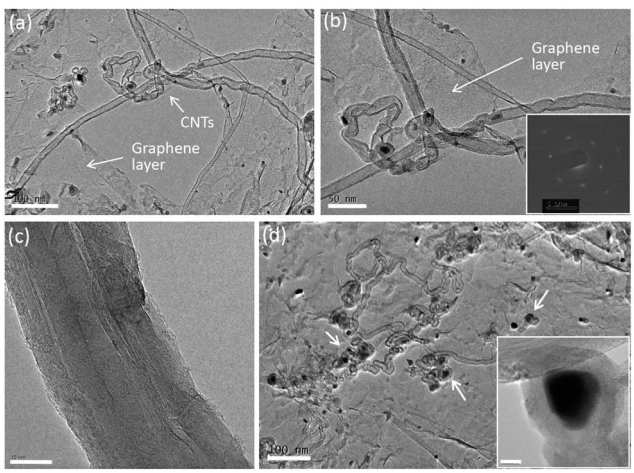

Fig. 3 TEM images of a piece of the CNT/G fiber (a and b), single grown CNT (c), and (d) CNT grown on graphene sheets with a short growth time (5 min). The inset in (b) shows the selected area electron diffraction of the graphene sheet. The inset in (d) shows an enlarged view of the catalyst. Scale bars: a, 100 nm; b, 50 nm; c, 10 nm; d, 100 nm; and inset of d, 10 nm.

ESI†). The catalyst was enwrapped in the carbon shells (Fig. 3d, inset), which may have contributed to the capacitance.

Fig. 4c shows the Raman spectrum of a CNT/G fiber in comparison with a pure graphene fiber (Fig. 4a) and a G/Fe_3O_4 fiber (Fig. 4b). As can be seen, all of them exhibit the typical D and G bands.[37] Both the graphene fiber (Fig. 4a) and the G/Fe_3O_4 fiber (Fig. 4b) derived from hydrothermally reduced graphene oxides show a relatively high D band with an intensity ratio (I_D/I_G) of *ca.* 0.9, which is much larger than the corresponding value of 0.39 for the CNT/G fiber (Fig. 4c). The relatively strong G band seen in Fig. 4c indicates a highly graphitic crystalline structure for the CNT/G fiber.

Fig. 5 represents the XRD patterns of a graphene fiber, G/Fe_3O_4 fiber, and CNT/G fiber, respectively. As can be seen, the graphene fiber has a diffraction peak at $2\theta \approx 25^\circ$ assigned to the (002) plane of stacked graphene sheets.[6] Apart from the typical peak at $2\theta \approx 25^\circ$, the G/Fe_3O_4 fiber exhibits a series of distinct diffraction peaks positioned at *ca.* 30.4°, 35.7°, 43.5°, 53.7°, 57.3° and 63° corresponding to the (220), (311), (400), (422), (511) and (440) planes of the intercalated Fe_3O_4 nanoparticles

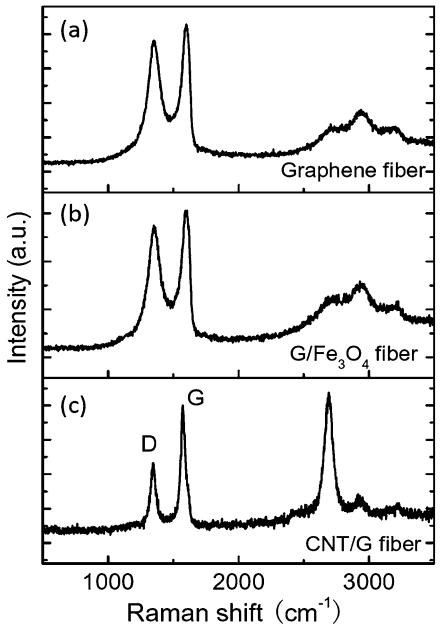

Fig. 4 Raman spectra of a graphene fiber (a), G/Fe_3O_4 fiber (b), and CNT/G fiber (c).

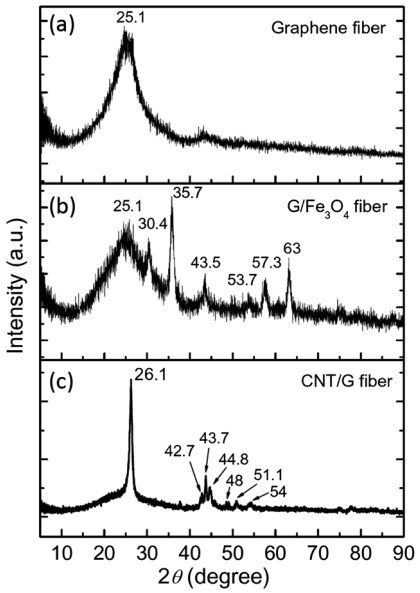

Fig. 5 XRD patterns of a graphene fiber (a), G/Fe_3O_4 fiber (b), and CNT/G fiber (c).

(JCPDS no. 88-0315).[38] In contrast, most of the diffraction peaks associated with Fe_3O_4 largely disappeared and the graphene peak at *ca.* 25° was drastically suppressed for the sample of CNT/G fiber (Fig. 5c). The peak at 26.1° corresponds to the (002) interplanar spacing between the CNT walls. The other CNT characteristic peaks at $2\theta = ca.$ 42.7° and 54° correspond to the (100) and (004) reflection, respectively.[39] On the other hand, the crystalline phase of Fe residue is represented by a strong (110) reflection at *ca.* 43.7° with an additional peak at 51.1°.[39] The remaining peaks at *ca.* 44.8° and 48° are presumably related to the iron carbide associated with the resultant CNTs.[39] These results indicate that the initially intercalated Fe_3O_4 nanoparticles within the graphene fibers have been reduced into Fe nanoparticles by the H_2 flow during the CVD process for the CNT growth (Fig. 3).

Having performed the structural characterization, we further investigated the cyclic voltammetry (CV) response of a single CNT/G fiber as the working electrode. A Pt wire and Ag/AgCl (3 M KCl) were used as the counter and reference electrodes, respectively. The electrolyte was 1 M Na_2SO_4 aqueous solution. As shown in Fig. 6a, the CNT/G fiber electrode exhibited rectangular CV curves, showing ideal capacitive behavior within the measured scan rates from 10 to 500 mV s^{-1} probably due to the fast ion transportation resulting from the high conductivity and high specific surface area of the CNT/G fiber.

Efficient ion adsorption/desorption on the CNT/G fiber was also evidenced by the linear relationship of the discharge current densities with the scan rates over 10–500 mV s^{-1} (Fig. 6b). In contrast, the pure graphene fiber exhibited the compressed current–voltage cycles with increased scan rates (Fig. S2†), indicating the ineffective ion transport through the neat graphene fiber. The galvanostatic charge–discharge curves at a current density of 10–200 μA cm^{-2} of the CNT/G fiber are shown in Fig. 6c. The fiber surface area (A) can be estimated from $A = 2\pi rL$, where r is the fiber radius and L is the fiber length. Based on the fiber surface area, the specific capacitance (C_s) calculated by using the slope of the discharge curves with different current densities is between 1.2 and 1.3 mF cm^{-2}, indicating the stable capacitance performance. These results show that the CNT and graphene hybrid microfibers with a large specific surface area greatly facilitate the rapid transport of electrolyte ions within the electrode material to show the improved electrochemical properties.

To explore the application of CNT/G fibers in flexible and wearable electronic devices, we fabricated the textile electrodes woven from CNT/G fibers. Due to the rough surface of the

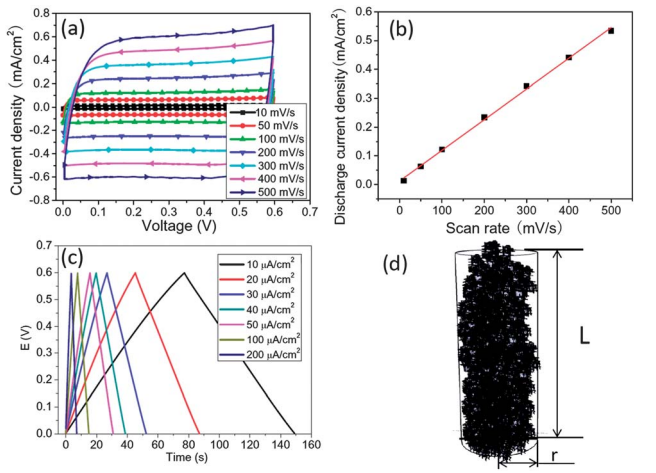

Fig. 6 (a) CV curves of the capacitors of the CNT/G fiber at scan rates of 10–500 mV s^{-1}. (b) Evolution of the discharge current density *versus* scan rate. (c) Galvanostatic charge–discharge cycles (CC) at current density of 10–200 μA cm^{-2} of the CNT/G fiber. (d) A schematic model for estimating the cylindrical surface area of the CNT/G fiber.

individual CNT/G fibers, it is difficult, if not impossible, to directly knit CNT/G fibers into textile. We therefore knitted the textile from G/Fe_3O_4 fibers (Fig. 7a) first, followed by the CVD growth of CNTs as mentioned in the Experimental section (Fig. 7b). The as-formed textile of the CNT/G fibers is still flexible just like that of the G/Fe_3O_4 fiber (insets in Fig. 7a and b). The overlapped CNT/G fibers (Fig. 7c) within the textile show the structural feature of highly entangled CNTs (Fig. 7d) similar to that of individual CNT/G fibers in Fig. 2h and i.

Fig. 8 shows a schematic structure of the flexible supercapacitor using the CNT/G fiber textiles as electrodes (Fig. 8a), and the final supercapacitors in the flat (Fig. 8b) and bending (Fig. 8c) states. A thin polyethylene terephthalate (PET) coated with Au was used as the supporting substrate and current collector. The separator is a filter paper soaked with 1 M Na_2SO_4 aqueous electrolyte. As shown in the insets of Fig. 8b and c, the charged device can light a commercial LED in either the flat or bending state, although the charge voltage is only 0.6 V.

To quantitatively investigate the electrochemical performance of the newly developed flexible supercapacitor, we measured both CV and charge–discharge curves (Fig. 9). As can be seen in Fig. 9a, the device maintained a nearly rectangular CV shape over a wide range of scan rates (0.01–10 V s^{-1}), showing a great capacitive behavior. The straight triangular charge–discharge curves are directly associated with the electrical double layer (Fig. 9b). The capacitance C_s defined as C/S (here, C is the capacitance and S is the total surface area of all CNT/G fibers within the textile electrodes) was calculated by using the slope of the discharge curves to be about 0.74 mF cm^{-2} at a current density of 10 μA cm^{-2}. This value exceeds that of the fiber-shaped solid supercapacitor based on ZnO nanowires and graphene films (0.4 mF cm^{-2}),[40] and is similar to that of the graphene-based fiber shaped EC.[41] The flexible supercapacitors also work well in a voltage range of 0–1.0 V (Fig. S3†). The capacitance was calculated by using the slope of the discharge curves to be about 0.98 mF cm^{-2} at a current density of 20 μA cm^{-2}, which is similar to that tested in a voltage range of 0–0.6 V. Accordingly, the weight-specific capacitances were determined to be about 200.4 F g^{-1} by use of the equations reported previously,[42–44] which is even higher than those of some typical graphene-based and CNT-based supercapacitors (Table S1†).[45–48]

The textile supercapacitors have similar CV curves in both the bending and flat states (Fig. 9c). A long-term bending cycle test on this textile supercapacitor showed an initial decrease in the capacitance, which then leveled off at a stable value of *ca.* 0.4 mF cm^{-2} after 1000 cycles (Fig. 9d). With the increase of the

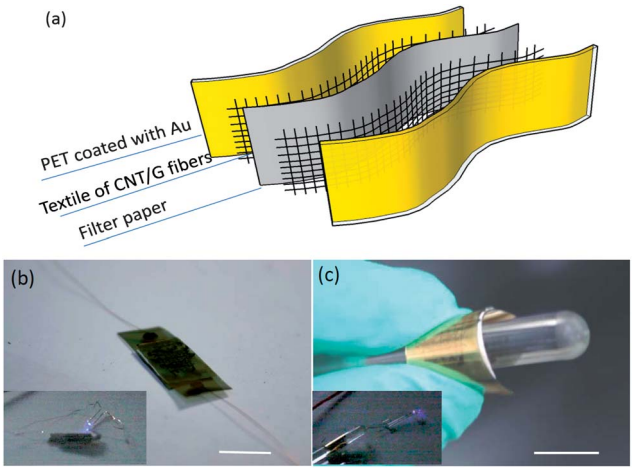

Fig. 8 (a) Schematic illustration of a flexible supercapacitor using the textile of CNT/G fibers as electrodes. (b and c) Photos of the fabricated textile supercapacitor in the flat and bending states, respectively. Insets of (b) and (c) show a light-emitting-diode (LED) lighted by this textile supercapacitor in the flat and bending states. Scale bar: b and c, 1 cm.

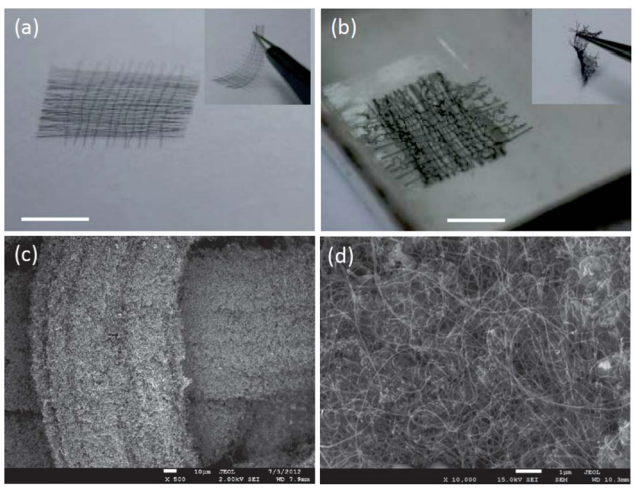

Fig. 7 Photographs of the G/Fe_3O_4 fiber textile (a) and the CNT/G fiber textile (b). Insets in (a) and (b) show the bent states. (c) SEM image of the overlaped CNT/G fibers within the textile, and (d) its enlarged surface. Scale bars: a and b, 0.5 cm; c, 10 μm; d, 1 μm.

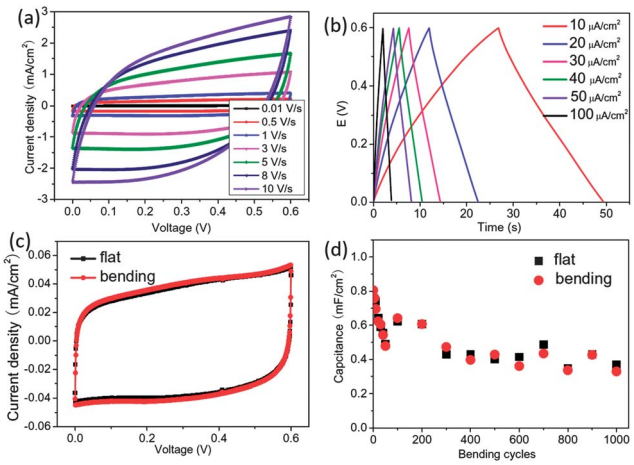

Fig. 9 (a) CV curves of the supercapacitor of the CNT/G fiber textile under the scan rate ranging from 0.01 to 10 V s^{-1}. (b) The galvanostatic charge–discharge curves at current density of 10–100 μA cm^{-2} of the CNT/G fiber textile supercapacitor. (c) CV curves of the CNT/G fiber textile supercapacitor in the flat and bending states for one typical bending cycle, respectively. The scan rate is 100 mV s^{-1}. (d) The durability test of the CNT/G fiber textile supercapacitor undergoing the repeated flat-to-bending cycles.

repeated flat-to-bending cycles, the rectangular CV curves shrink gradually and finally stabilize after about 200 bending cycles (Fig. S4†), which is consistent with the capacitance variation in Fig. 9d. The initial capacitance drop could also be explained by the fact that the CNT/G fiber has the increased resistance during the early stage bending process, most probably due to the deformation of the CNT/G fiber (Fig. S5†). The increased resistance could reduce the capacitive performance to some extent.

4 Conclusions

In summary, we have fabricated the new CNT/G hybrid fibers with a high surface area and electrical conductivity by pre-intercalating Fe_3O_4 nanoparticles into graphene fibers for subsequent CVD growth of CNTs. A flexible textile of CNT/G fibers was also prepared and used as electrodes for the construction of flexible supercapacitors. Apart from the textile supercapacitors demonstrated in this study, the CNT/G hybrid fibers could find many more applications in different fields, including catalysis, separation, and adsorption.

Acknowledgements

This work was supported by the National Basic Research Program of China (2011CB013000), NSFC (21004006, 21174019 and 51161120361), Fok Ying Tong Education Foundation (131043), the 111 Project B07012, NCET-10-0047, SRF for ROCS, SEM (20100732002), research foundation for the doctoral program of higher education of China (20101101120036), NSFC-NSF (1106160) and AFOSR (FA9550-12-1-0037).

Notes and references

1 A. K. Geim and K. S. Novoselov, *Nat. Mater.*, 2007, **6**, 183.
2 K. S. Novoselov, A. K. Geim and S. V. Morozov, *Science*, 2004, **306**, 666.
3 K. S. Novoselov, A. K. Geim and S. V. Morozov, *Nature*, 2005, **438**, 197.
4 Y. B. Zhang, Y. W. Tan, H. L. Stormer and P. Kim, *Nature*, 2005, **438**, 201.
5 A. A. Balandin, S. Ghosh, W. Z. Bao, I. Calizo, D. Teweldebrhan, F. Miao and C. N. Lau, *Nano Lett.*, 2008, **8**, 902.
6 Y. X. Xu, K. X. Sheng, C. Li and G. Q. Shi, *ACS Nano*, 2010, **4**, 4324.
7 Z. H. Tang, S. L. Shen, J. Zhuang and X. Wang, *Angew. Chem., Int. Ed.*, 2010, **49**, 4603.
8 Z. Xu and C. Gao, *Nat. Commun.*, 2011, **2**, 571, DOI: 10.1038/ncomms1583.
9 H. P. Cong, X. C. Ren, P. Wang and S. H. Yu, *Sci. Rep.*, 2012, **2**, 613, DOI: 10.1038/srep00613.
10 Z. L. Dong, C. C. Jiang, H. H. Cheng, Y. Zhao, G. Q. Shi, L. Jiang and L. T. Qu, *Adv. Mater.*, 2012, **24**, 1856.
11 C. G. Hu, Y. Zhao, H. H. Cheng, Y. Wang, Z. L. Dong, C. C. Jiang, X. Q. Zhai, L. Jiang and L. T. Qu, *Nano Lett.*, 2012, **12**, 5879.
12 X. Wang, L. J. Zhi, N. Tsao, Z. Tomovic, J. L. Li and K. Mullen, *Angew. Chem., Int. Ed.*, 2008, **47**, 2990.
13 X. Y. Yang, X. Dou, A. Rouhanipour, L. J. Zhi, H. J. Rader and K. Mullen, *J. Am. Chem. Soc.*, 2008, **130**, 4216.
14 L. T. Qu, Y. Liu, J. B. Baek and L. M. Dai, *ACS Nano*, 2010, **4**, 1321.
15 D. S. Yu, Y. Yang, M. Durstock, J. B. Baek and L. M. Dai, *ACS Nano*, 2010, **4**, 5633.
16 K. P. Gong, F. Du, Z. H. Xia, M. Durstock and L. M. Dai, *Science*, 2009, **323**, 760.
17 L. T. Qu, F. Du and L. M. Dai, *Nano Lett.*, 2008, **8**, 2682.
18 D. Y. Cai, M. Song and C. X. Xu, *Adv. Mater.*, 2008, **20**, 1706.
19 V. C. Tung, L. M. Chen, M. J. Allen, J. K. Wassei, K. Nelson, R. B. Kaner and Y. Yang, *Nano Lett.*, 2009, **9**, 1949.
20 A. P. Yu, P. Ramesh, X. B. Sun, E. Bekyarova, M. E. Itkis and R. C. Haddon, *Adv. Mater.*, 2008, **20**, 4740.
21 Q. Su, Y. Y. Liang, X. L. Feng and K. Mullen, *Chem. Commun.*, 2010, **46**, 8279.
22 Z. J. Fan, J. Yan, L. J. Zhi, Q. Zhang, T. Wei, J. Feng, M. L. Zhang, W. Z. Qian and F. Wei, *Adv. Mater.*, 2010, **22**, 33.
23 Y. W. Cheng, S. T. Lu, H. B. Zhang, C. V. Varanasi and J. Liu, *Nano Lett.*, 2012, **12**, 4206.
24 F. Du, D. S. Yu, L. M. Dai, S. Ganguli, V. Varshney and A. K. Roy, *Chem. Mater.*, 2011, **23**, 4810.
25 M. K. Shin, B. Lee, S. H. Kim, J. A. Lee, G. M. Spinks, S. Gambhir, G. G. Wallace, M. E. Kozlov, R. H. Baughman and S. J. Kim, *Nat. Commun.*, 2012, **3**, 650, DOI: 10.1038/ncomms1661.
26 P. C. Chen, G. Shen, S. Sukcharoenchoke and C. Zhou, *Appl. Phys. Lett.*, 2009, **94**, 043113.
27 X. L. Wu, L. Y. Jiang, F. F. Cao, Y. G. Guo and L. J. Wan, *Adv. Mater.*, 2009, **21**, 2710.
28 W. Sun and X. Y. Chen, *J. Power Sources*, 2009, **193**, 924.
29 Y. P. Zhang, H. B. Li, L. K. Pan, T. Lu and Z. Sun, *J. Electroanal. Chem.*, 2009, **634**, 68.
30 P. Y. Simon and Y. Gogotsi, *Nat. Mater.*, 2008, **7**, 845.
31 P. J. Hall, M. Mirzaeian, S. I. Fletcher, F. B. Sillars, A. J. R. Rennie, G. O. Shitta-Bey, G. Wilson, A. Cruden and R. Carter, *Energy Environ. Sci.*, 2010, **3**, 1238.
32 D. Pech, M. Brunet, H. Durou, P. H. Huang, V. Mochalin, Y. Gogotsi, P. L. Taberna and P. Simon, *Nat. Nanotechnol.*, 2010, **5**, 651.
33 J. Bae, M. K. Song, Y. J. Park, J. M. Kim, M. L. Liu and Z. L. Wang, *Angew. Chem., Int. Ed.*, 2011, **50**, 1683.
34 Y. Zhao, C. G. Hu, Y. Hu, H. H. Cheng, G. Q. Shi and L. T. Qu, *Angew. Chem., Int. Ed.*, 2012, **124**, 11533.
35 Y. Zhao, J. Liu, Y. Hu, H. H. Cheng, C. G. Hu, C. C. Jiang, L. Jiang, A. Y. Cao and L. T. Qu, *Adv. Mater.*, 2013, **25**, 591.
36 A. Peigney, C. Laurent, E. Flahaut, R. R. Bacsa and A. Rousset, *Carbon*, 2001, **39**, 507.
37 H. H. Cheng, Y. Zhao, Y. Q. Fan, X. J. Xie, L. T. Qu and G. Q. Shi, *ACS Nano*, 2012, **6**, 2237.
38 H. J. Liu, J. H. Wu, J. H. Min and Y. K. Kim, *J. Alloys Compd.*, 2012, **537**, 60.
39 G. E. Grechnev, V. A. Desnenko, A. V. Fedorchenko, A. S. Panfilov, Y. A. Kolesnichenko, L. Y. Matzui,

M. I. Grybova, Y. I. Prylutskyy, U. Ritter and P. Scharff, *Low Temp. Phys.*, 2010, **36**, 1086.
40 J. Bae, Y. J. Park, M. Lee, S. N. Cha, Y. J. Choi, C. S. Lee, J. M. Kim and Z. L. Wang, *Adv. Mater.*, 2011, **23**, 3446.
41 Y. Li, K. Sheng, W. Yuan and G. Q. Shi, *Chem. Commun.*, 2013, **49**, 291.
42 L. Zhang and G. Q. Shi, *J. Phys. Chem. C*, 2011, **115**, 17206.
43 K. P. Wang and H. Teng, *Carbon*, 2006, **44**, 3218.
44 C. J. Yu, C. Masarapu, J. P. Rong, B. Q. Wei and H. Q. Jiang, *Adv. Mater.*, 2009, **21**, 4793.
45 Z. Q. Niu, J. Chen, H. H. Hng, J. Ma and X. D. Chen, *Adv. Mater.*, 2012, **24**, 4144.
46 X. T. Zhang, Z. Y. Sui, B. Xu, S. F. Yue, Y. J. Luo, W. C. Zhan and B. Liu, *J. Mater. Chem.*, 2011, **21**, 6494.
47 L. L. Zhang and X. S. Zhao, *Chem. Soc. Rev.*, 2009, **38**, 2520.
48 Y. Q. Sun, Q. Wu and G. Q. Shi, *Energy Environ. Sci.*, 2011, **4**, 1113.

